H_2 Reduction Annealing Induced Phase Transition and Improvements on Redox Durability of Pt Cluster Decorated Cu@Pd electrocatalysts in Oxygen Reduction Reaction

Authors: Dinesh Bhalothia,[a,b] Cheng-Yang Lin,[a] Che Yan,[b] Ya-Tang Yang,[a*] and Tsan-Yao Chen[b,c,d*]

Affiliations:

[a.] Institute of Electronics Engineering, National Tsing Hua University, Hsinchu 30013, Taiwan

[b.] Department of Engineering and System Science, National Tsing Hua University, Hsinchu 30013, Taiwan

[c.] Institute of Nuclear Engineering and Science, National Tsing Hua University, Hsinchu 30013, Taiwan

[d.] Hierarchical Green-Energy Materials (Hi-GEM) Research Center, National Cheng Kung University, Tainan 70101, Taiwan

Corresponding Authors:

Tsan-Yao Chen

Email: chencaeser@gmail.com

Tel: +886-3-5715131 # 34271

FAX: +885-3-5720724

S1 Degradation pathways of carbon supported Pt-based nanocatalysts (NCs) during oxygen reduction reaction in fuel cell redox cycle.

Activity is not only one factor linked with the efficiency of nanocatalysts (NCs). NCs are expected to maintain their decisive features during the complete lifecycle of several thousands of hours. Especially at the cathode side, where the catalyst is exposed to the most drastic operating conditions, the stability of catalyst is a crucial prerequisite for high-performance fuel cells. Limited electrochemical stability of the current carbon supported cathodic NCs during oxygen reduction reaction in fuel cell redox cycle is one of the major bottleneck in the development of fuel cells. **Scheme S1** shows the detailed schematic for the degradation of Pt/C catalyst. The duty cycles of repeated start-ups and shut-downs were found to be extremely harmful to the catalyst and often have a dominant influence on its durability.[1-3] The main reason for catalyst degradation is that, the fuel cell undergoes high potentials during initial phase that lead to carbon and Pt degradation processes. As shown in **Scheme S1**, there are five major pathways responsible for NC degradation in the redox cycles. They are (1) Carbon support oxidation or decomposition/corrosion to CO_2 during electrochemical reactions at the NC interface. Carbon corrosion is very detrimental to long term fuel cell durability. Following reaction is responsible for such decomposition

$$C + 2H_2O \rightarrow Co_2 + 4H^+ + 4e^- \ldots\ldots\ldots\ldots\ldots\ldots\ldots\ldots\ldots\ldots equ\ S1$$

Factors including the presence of platinum, vigorous moist environment, temperature and the amount of carbon exposure will all play an influential role in carbon corrosion, (2) catalysts detachment, (3) Pt is dissolved and/or sintered into bigger agglomerates. Meanwhile, the agglomeration process is accelerated by carbon corrosion in oxidative conditions. As a result, NCs are detached from their support and tend to gather together, which results in the lower fuel cell performance, (4) NC agglomeration by interfacial atomic diffusion between nanoparticles and (5) Platinum nanoparticle dissolution and/or agglomeration will also occur during long periods of fuel cell operation. Nano sized platinum particles have very high surface energies that promote their

migration and agglomeration into larger particles in order to reduce the surface energy of these materials. This phenomenon is commonly referred to as ostwald ripening. NC growth through metal corrosion followed by re-deposition of metal ions to neighboring NCs from residual metal ions in the electrolyte or diffusion in the carbon surfaces. Surface poisoning or passivation by strongly bonded molecules at NC surfaces is also cause performance loss. Therefore, more durable, efficient, and inexpensive fuel cell electrocatalysts are desperately required before fuel cells can become commercially viable.

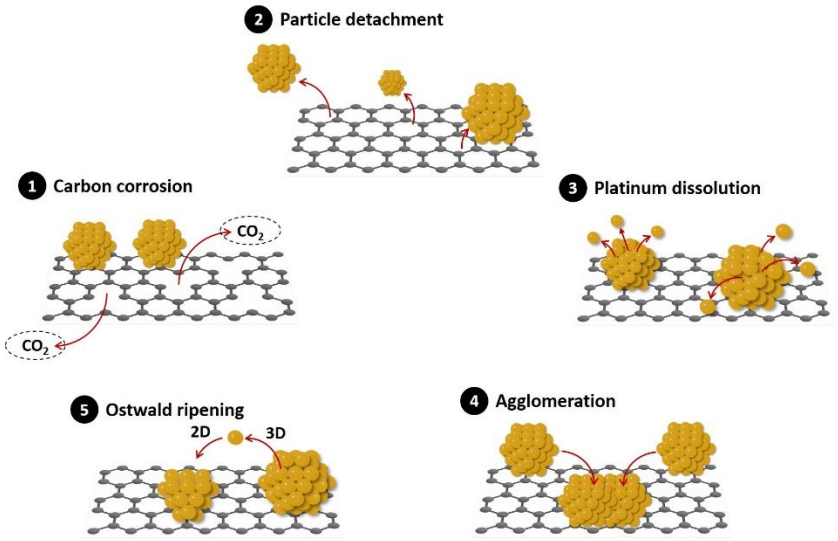

Scheme 1. Schematic pathways for degradation of cathodic NCs during oxygen reduction reaction in fuel cell redox cycle

S2 HRTEM image Pt-CNT.

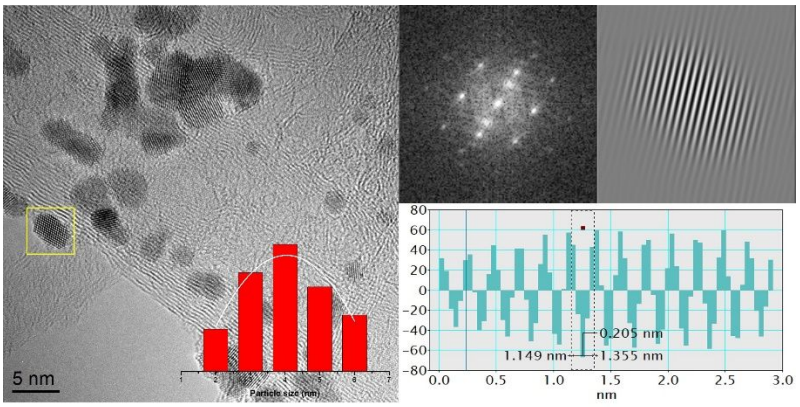

Figure S1. HRTEM image Pt-CNT. d-spacing values is calculated by using Inverse Fourier Transformed (IFT) images and their corresponding line histograms (insets). Fourier transformation pattern of selected area in HRTEM image is shown in corner.

S3 Comparative XRD analysis of Cu@Pd/Pt-H NC with control samples.

As depicted in **Figure S2**, peaks X1 and X2 refer to diffraction lines of (111) and (200) facets of metallic Pt phase in Pt-CNT crystal. For Pd-CNT, the asymmetry peak profile accounted for formation of PdO phase. In case of Pd@Pt NC, compared to that of Pd-CNT, larger extent of peak upshift at X1 and X2 reveals the higher extent of Pd-to-Pt intermix at (111) and (200) facets. Such an uneven intermix is understandable due to easy intercalation of Pt atoms in opened surfaces. Meanwhile, broadened peak with increased background diffusion scattering hump at peak region are caused by increasing surface roughness of NC. Such phenomena explain the intercalation of atomic Pt clusters into near-surface region of Pd@Pt NC. For Cu@Pt, significant suppression on peak intensities indicate the strong confinement effect on Cu crystal growth by adjacent to Pt crystal. The splitting of main diffraction line indicates the formation of Cu_3Pt alloy.

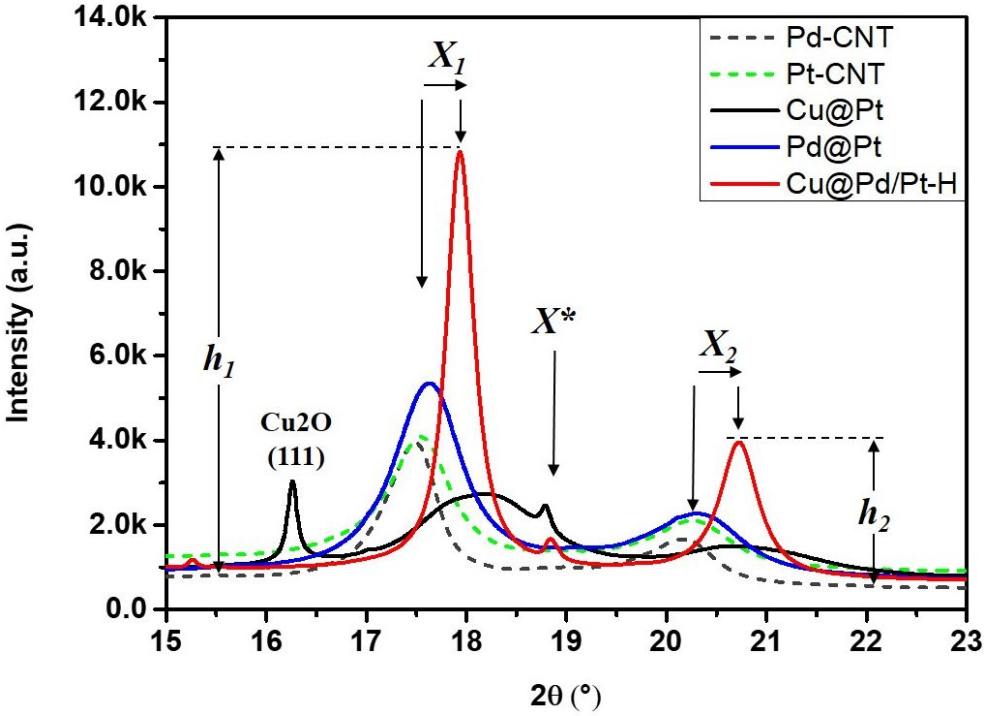

Figure S2. Comparative XRD patterns of Cu@Pd/Pt-H with control samples. All the spectra were measured under the incident X-ray of 18KeV.

S4 X-ray absorption spectroscopy inspection

As shown in **Figure S3**, compared to Pt foil, Pt-CNT has slightly decreased H_A and reduced H_B intensities. On the one hand, the decrease of HA indicates a suppressed surface oxygen chemisorption due to the absence of stabilization agent. On the other hand, reduced H_B represents the presence of disordered defects in NC surface. At the same time, inflection points for the peak maximum (arrow A) at 1st deviation spectra of Pt-CNT and Pt foil are located in the same place. Such a characteristic depicts the identical chemical state of the two samples.

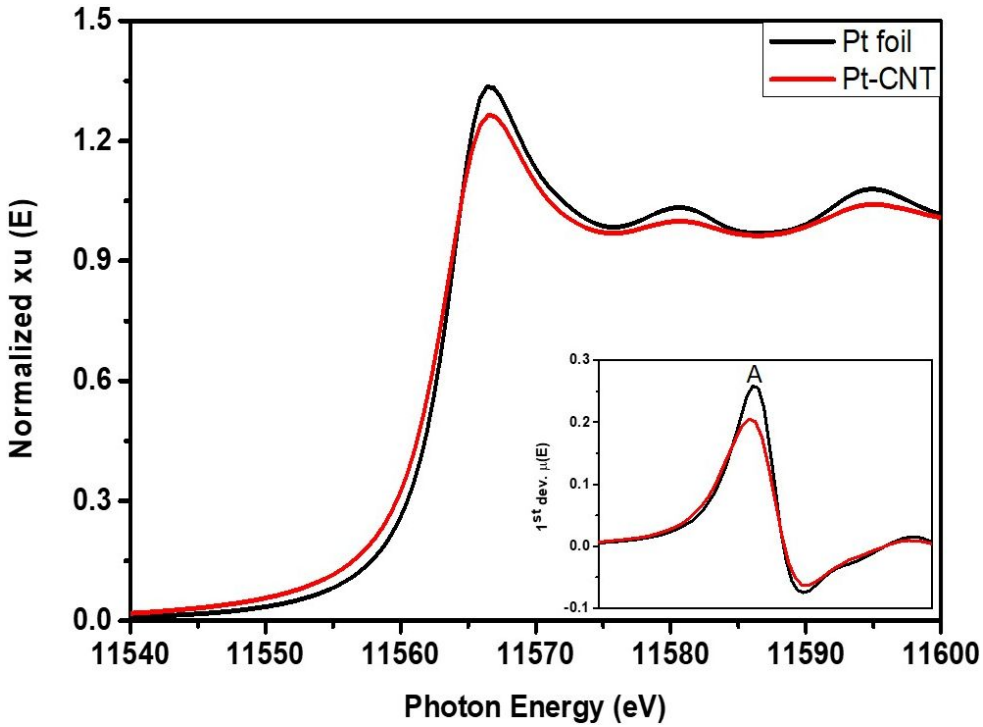

Figure S3. Pt L3-edge XANES spectra of Pt-CNT and standard Pt foil

S5 Comparative electrochemical and long term stability analysis of Cu@Pd/Pt-H NC with Cu@Pt and Pd@Pt NCs.

Figure S4 demonstrates cyclic voltammetry (CV) and linear sweep voltammetry (LSV) spectra of the experimental NCs (Cu@Pt, Pd@Pt and Cu@Pd/Pt-H) compared with that of J.M.-Pt/C. Herein, the CV curves were recorded in N_2-purged 0.1 M KOH solutions at 20mV/s under room temperature, whereas LSV curves were obtained in an O2-saturated KOH solution (0.1 M) at the rotation speed of working electrode is 1600 rpm. Corresponding electrochemical parameters have been summarized in **Table S1**.

Table S1. Comparative electrochemical performances of experimental NCs in ORR.

NC	n	ECSA $cm^2\ mg_{Pt+Pd}^{-1}$	E_{onset} V vs RHE	$JK_{0.85}$ mA cm^{-2}	$S.A._{0.85}$ mA cm^{-2}	$M.A._{0.85}$ mA mg_{Pt}^{-1}
Cu@Pt	4.2	617.7	0.885	2.84	0.033	20.4
Pd@Pt	3.5	300.8	0.955	8.19	0.108	91.3
Cu@Pd/Pt-H	3.7	204.0	0.898	16.3	0.536	308.2
J.M.-Pt/C	4.0	257.0	0.915	5.3	0.261	67.0

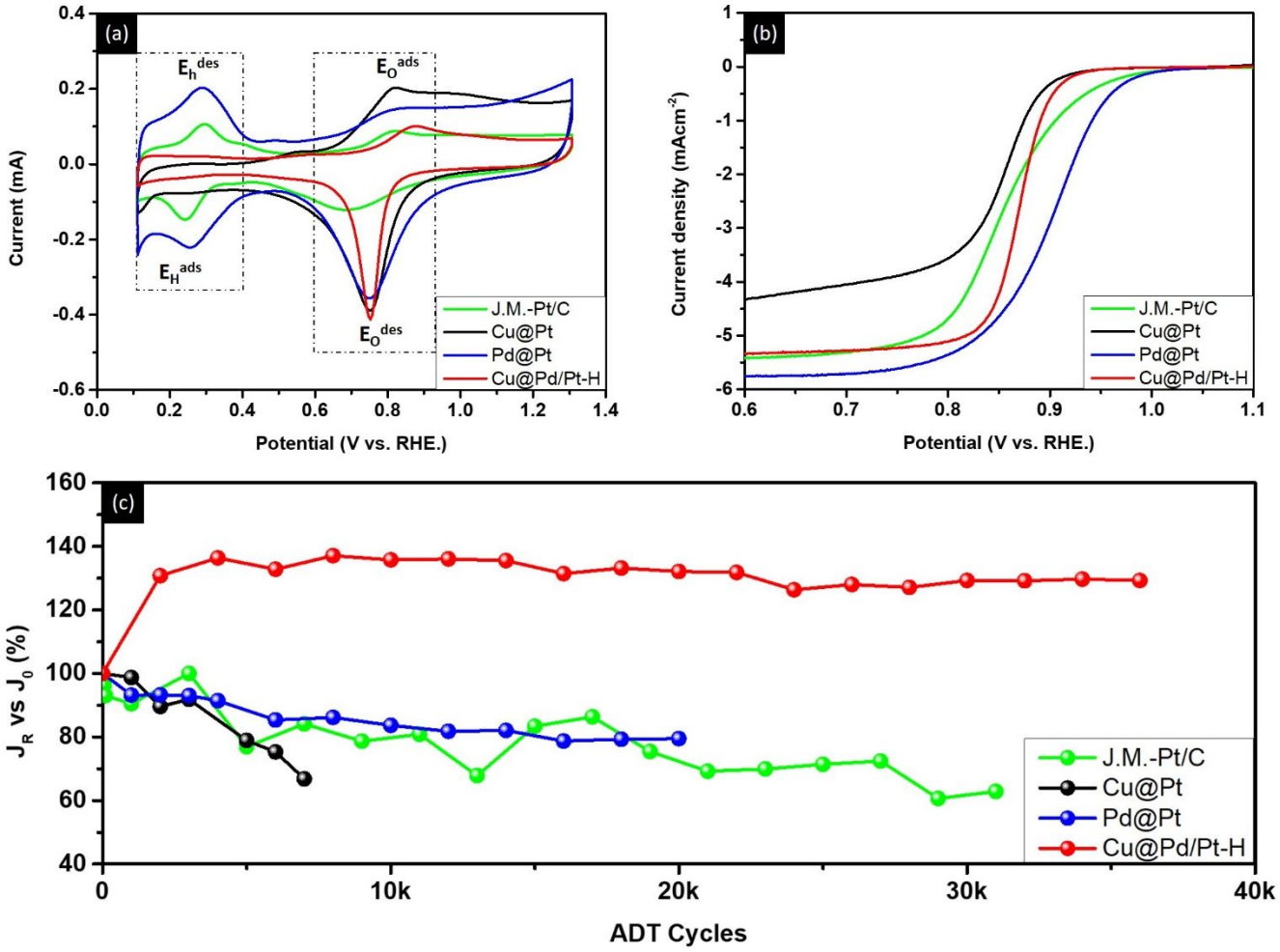

Figure S4. Comparative (a) CV and (b) LSV curves of Cu@Pd/Pt-H, J.M.-Pt/C, Cu@Pt and Pd@Pt. (c) Normalized initial and final current densities for experimental NCs compared with J.M.-Pt/C after different ADT cycles.

S6 CV sweeping and LSV curves of pristine and post annealed NCs during ADT cycles.

Figure S5 (a) and (c) demonstrates CV sweeping curves of Cu@Pd/Pt-H and Cu@Pd/Pt after different ADT cycles respectively. For Cu@Pd/Pt-H highly symmetric redox peaks with reference of position and intensity indicate the reversible chemical states in CV cycles. Here changing in peak position and intensity symmetrically with increasing ADT cycles confirm its strong electrochemical stability in long-term ORR. Whereas, for Cu@Pd/Pt, i.e. before annealing asymmetry in position and intensity of peaks refers decreased durability due to less utilization of Pt metal.

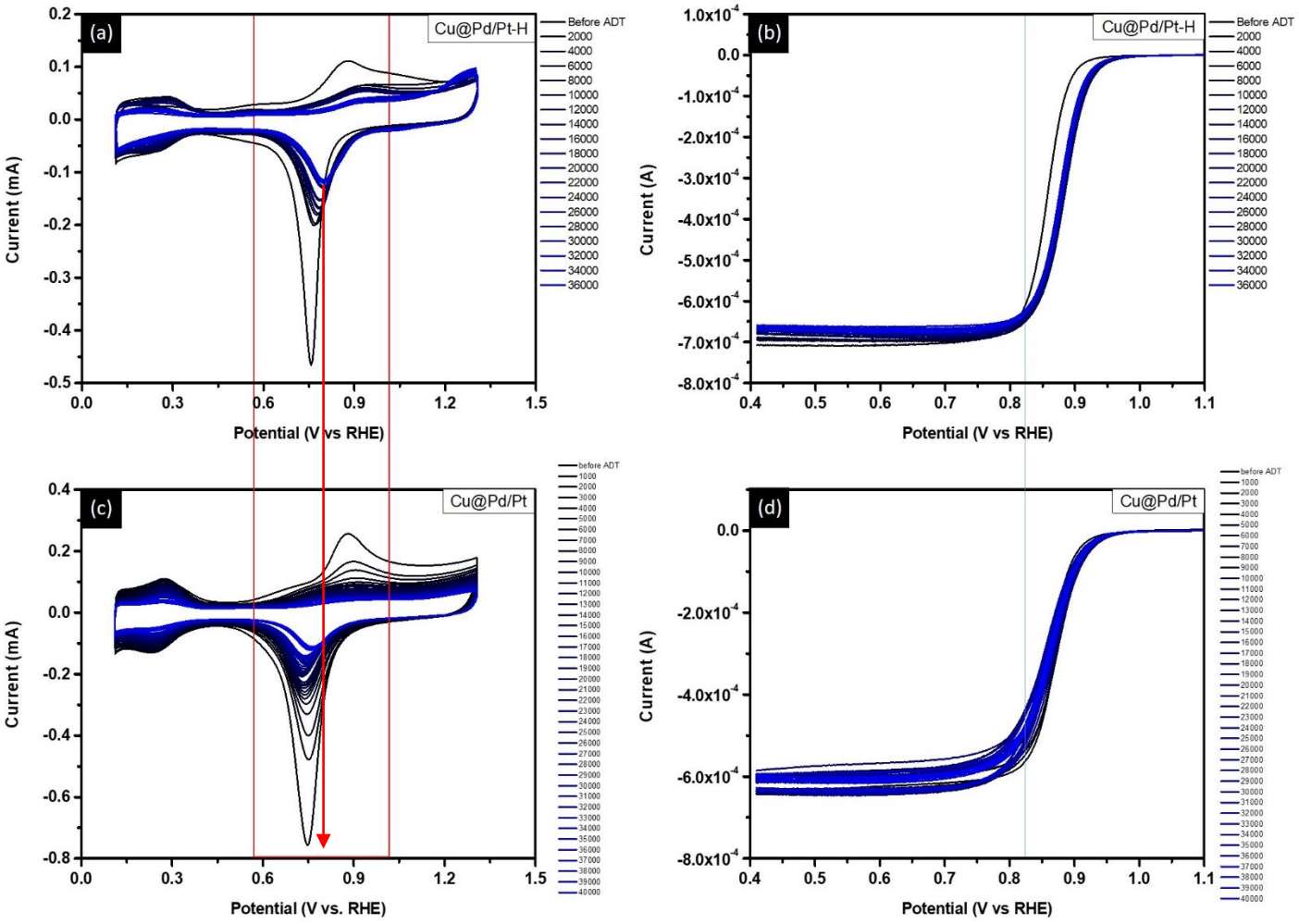

Figure S5. CV sweeping curves of (a) Cu@Pd/Pt-H and (c) Cu@Pd/Pt. Changes in LSV curves of (b) Cu@Pd/Pt-H and (d) Cu@Pd/Pt.

S7 TEM and EDX results for Cu@Pd/Pt and Cu@Pd/Pt-H samples before and after ADT

TEM images and corresponding EDX results for post-ADT Cu@Pd/Pt-H and Cu@Pd/Pt are respectively presented in **Figure S6a** and **Figure S6b**. As can be seen, Cu@Pd/Pt possesses higher extent of agglomeration between NCs as compared to that of Cu@Pd/Pt-H. Such a characteristic can be attributed to the presence of high content surface defect in Cu@Pd/Pt. In ADT measurements, applied potential cycles triggers the oxidation and reduction cycles in NC surface. This scenario results in high extent of atomic diffusion for reducing surface energy as a result of agglomeration of NCs. Meanwhile, without formation of CuPd and PtCu alloys, severe Pd corrosion (suppression of Pd content in EDX, **Table S2**) is found which is the main reason for the suppression of ORR activity for Cu@Pd/Pt in ADT. On the other hand, compared to those of Cu@Pd/Pt, interparticle agglomeration and Pd corrosion are suppressed and can be attributed to the improved stability of Cu@Pd/Pt-H in ORR (Figure R3a).

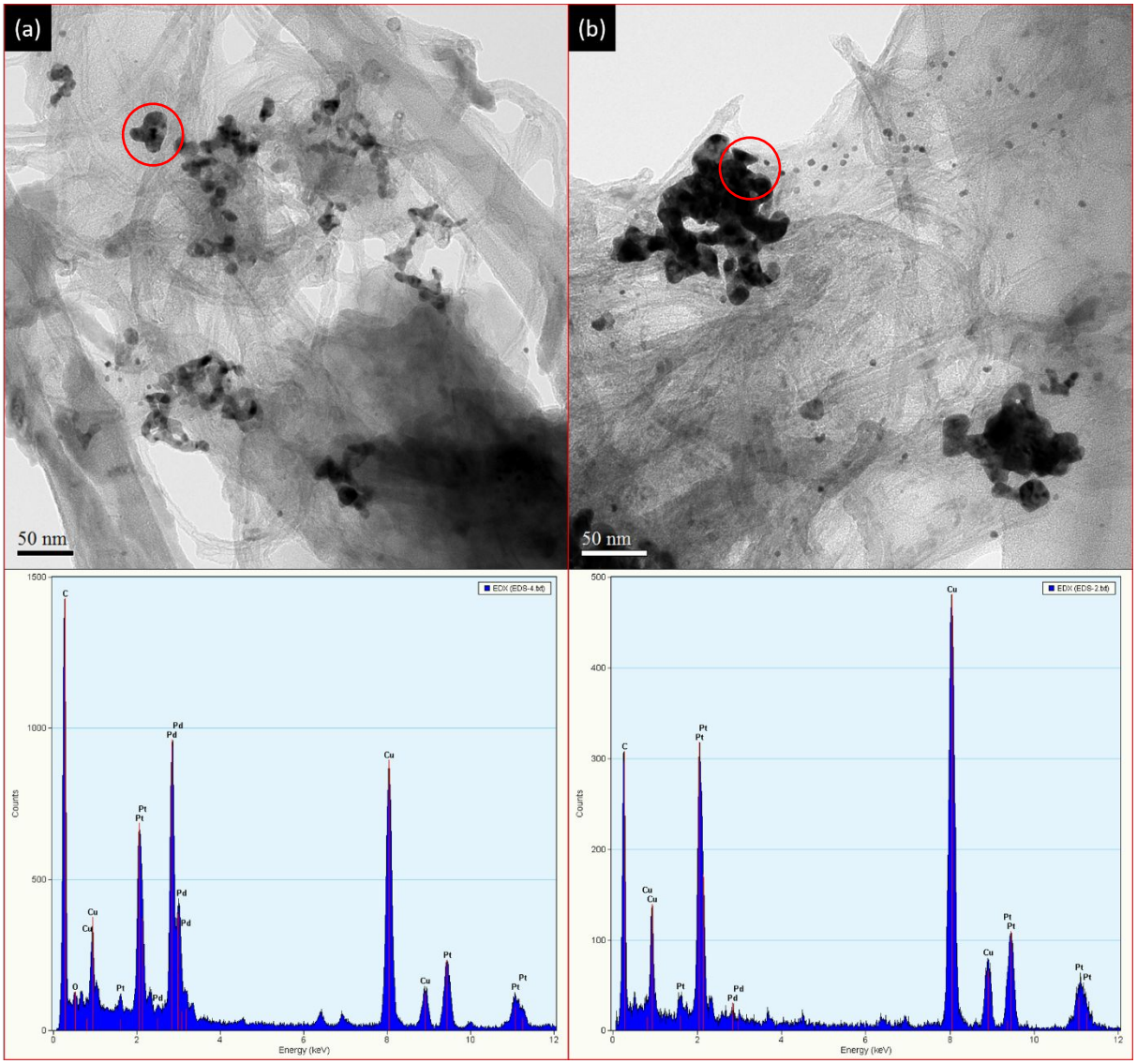

Figure S6 TEM images of (a) Cu@Pd/Pt-H and (b) Cu@Pd/Pt after ADT. The EDX results are measured in the region marked by hollow cycles.

Table S2 EDX results of Post-ADT Cu@Pd/Pt-H and Cu@Pd/Pt NCs in atomic ratios.

NC	Cu	Pd	Pt
Cu@Pd/Pt-H	51.1	31.8	17.1
Cu@Pd/Pt	77.3	15.8	6.8

S7 References:

1. Mench, M. M.; Kumbar, E. C.; Veziroglu, T. N. *Polymer Electrolyte Fuel Cell Degradation*; Academic Press Elsevier: Waltham, 2012.

2. Borup, R.; Meyers, J.; Pivovar, B.; Kim, Y. S.; Mukundan, R.; Garland, N.; Myers, D.; Wilson, M.; Garzon, F.; Wood, D.; Zelenay, P.; More, K.; Stroh, K.; Zawodinski, T.; Boncella, J.; McGrath, J. E.; Inaba, M.; Miyatake, K.; Hori, M.; Ota, K.; Ogumi, Z.; Miyata, S.; Nishikata, A.; Siroma, Z.; Uchimoto, Y.; Yasuda, K.; Kimijima, K.; Iwashita, N. Scientific aspects of polymer electrolyte fuel cell durability and degradation. *Chem. Rev*. **2007**, 107, 3904−3951

3. Zhang, S.; Yuan, X.; Hin, J. N. C.; Wang, H.; Friedrich, K. A.; Schulze, M. A review of platinum-based catalyst layer degradation in proton exchange membrane fuel cells *J. Power Sources.* **2009**, 194, 588−600.